# Continuous wave supercontinuum generation pumped in the normal group velocity dispersion regime on a highly nonlinear fiber

**Margarida Facão,[1,*] Maria Inês Carvalho,[2] Gil Martins Fernandes,[3,4] Ana Maria Rocha,[4] and Armando Nolasco Pinto[3,4]**

[1]*Departamento de Física, Universidade de Aveiro and I3N, Aveiro 3810-193, Portugal*
[2]*DEEC/FEUP and INESC TEC, Universidade do Porto, Rua Dr Roberto Frias, Porto 4200-465, Portugal*
[3]*Departamento de Electrónica, Telecomunicações e Informática, Universidade de Aveiro, Aveiro 3810-193, Portugal*
[4]*Instituto de Telecomunicações, Aveiro 3810-193, Portugal*
**Corresponding author: mfacao@ua.pt*

Received December 10, 2012; accepted January 28, 2013;
posted February 6, 2013 (Doc. ID 181399); published March 18, 2013

We have obtained spectral broadening by pumping a nonmicrostructured highly nonlinear fiber with a continuous wave signal from a Raman fiber laser. The experiment was simulated using a generalized Schrödinger equation containing the actual Raman response of the fiber as calculated from the experimental Raman gain. A different input-noise model, that reproduces well the power spectral density of the laser, was used and compared with others previously proposed. © 2013 Optical Society of America

*OCIS codes:* 060.4370, 060.3510, 190.5650.

## 1. INTRODUCTION

The phenomenon of supercontinuum generation (SCG) consists of an extremely wide spectral broadening of a light signal during its propagation on a nonlinear medium. The research on SCG in optical fibers has started in the early 1970s [1] but only in the late 1990s, with the advent of photonic crystal fibers (PCFs) and the possibility of designing dispersion and obtaining high nonlinearities according to the available laser pumps, has it reappeared with all its strength. Despite the intense research that followed these new SC experiments using PCFs [2], it still attracts much attention from fundamental and applied viewpoints [3–5]. Moreover, the ultrawideband spectrum generated by the SC has been successfully utilized in several applications, such as optical frequency metrology [6], generation of ultrashort optical pulses [7], photonic time stretch analog-to-digital conversion [8], spectroscopy [9], and optical coherence tomography [10].

The SCG has been obtained from ultrashort pulses in the femtosecond regime, from long pulses that are typically in the picosecond regime or even from continuous wave (CW) signals. In the femtosecond regime, the pulses are usually launched in the anomalous region of dispersion and the SC is mainly the consequence of fission of higher-order solitons followed by soliton self-frequency shift, and amplification of dispersive waves [11,12]. In the CW regime and anomalous group velocity dispersion (GVD), the first stages of spectral broadening are achieved by modulational instability (MI) that is equivalent to a noise-induced four-wave mixing (FWM). The MI is responsible for the breakup of the CW into solitons, and from that stage on the mechanisms are identical to the ones in femtosecond pumping [13–15]. In both the anomalous and normal GVD, the CW signals may develop a Stokes spectral band caused by stimulated Raman scattering (SRS) seeded from noise [16].

Only a few kinds of pulsed lasers are able to generate several watts of average output powers. On the other hand, modern CW lasers such as cascaded Raman fiber lasers can generate signals with several watts and can be easily fabricated. The CW lasers do not benefit from the high peak-to-average power ratio of pulsed lasers; therefore, longer interaction lengths are required to produce SC, even when highly nonlinear fibers (HNLFs) are used [17]. In the ultrashort pulsed case, a few meters is usually sufficient and the produced SC is much wider and much more coherent than in the CW pumping schemes. However, for similar spectral widths, CW SC have a higher average power and exhibit a higher power spectral density than pulsed SC [15].

Here, we have used a cascaded Raman fiber laser to pump in the normal GVD region of a nonmicrostructured HNLF. To further study the observed spectral broadening and anticipate better experimental configurations, we have also done a careful numerical simulation. Even though the challenges of simulating the dispersive and nonlinear propagation of pulses in optical fibers are reasonably standard using a generalized nonlinear Schrödinger equation (GNLSE), the propagation of CW signals is not yet well studied. The GNLSE is also suited for CW propagation; however the CW signal has to be temporally truncated in order to fit in the numerical window and a proper averaging has to be made if we want to simulate the integration times of the optical spectrum analyzers. Moreover, since the nonlinear effects that lead to the SCG in the CW regime are essentially noise seeded, an adequate noise input model is also indispensable. Several attempts to do so have been previously considered, namely, the addition of one

 

photon per mode [14], the consideration of random spectral phase [15], or random phase noise [13,18,19]. Other models, that are computationally more demanding, simulate the actual laser system in order to obtain the temporal output profile as the simulation of a cascaded ASE source [5] or an ytterbium fiber laser [20]. The main contributions of our work are the numerical simulations that use a new noise input model with both random spectral amplitude and phase following the approach presented in [21]. Moreover, the Raman gain of the fiber was measured and the respective Raman response function was used in the numerical simulations.

This paper is organized in four sections. In Section 2, we present the experimental setup and results. In Section 3, we present the propagation equation and numerical methods used, and in Section 4 we present the simulation results corresponding to the experimental results but also for higher pump powers. Finally, we conclude in Section 5.

## 2. EXPERIMENTAL RESULTS

The experimental setup used to generated SC is schematically shown in Fig. 1. In this experimental setup, a continuous signal from a Raman fiber laser (IPG, model RLR-10-1480) emitting at 1480 nm, with a depolarized single mode output and a maximum optical power of 10 W, is launched into 800 m of HNLF whose zero-dispersion wavelength (ZDW) is at 1531 nm, with a dispersion slope of 0.01818 ps km$^{-1}$ nm$^{-2}$, nonlinear coefficient $\gamma = 10.5$ W$^{-1}$ km$^{-1}$, as measured using the technique referred to in [22], and an attenuation of $\alpha_{\mathrm{dB}} = 3.15$ dB/km at 1495 nm. The spectrum of the Raman fiber laser for 1 W is shown in Fig. 2. The zero-dispersion wavelength, the dispersion slope and the attenuation of the fiber were measured with an Optical Network Analyzer, 86038-90B01 from Agilent.

The output spectra was measured by an Optical Spectrum Analyser (OSA), Advantest Q8384 from Agilent, after being attenuated by 10 dB. The results for different input power levels are shown in Fig. 3. Due to power limitations of the OSA and

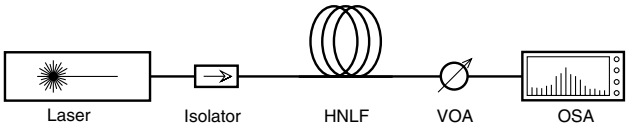


Fig. 1. Experimental setup.

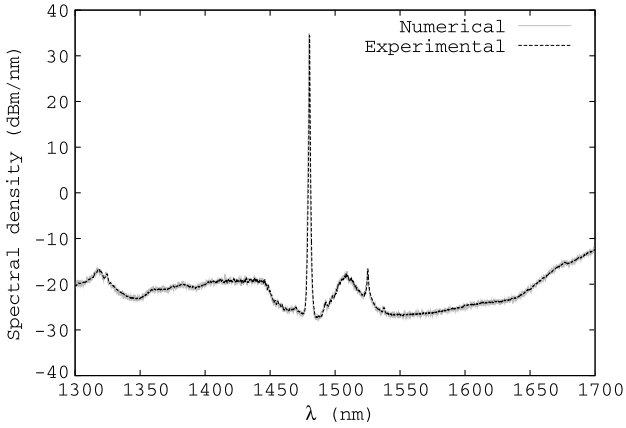


Fig. 2. Power spectrum density of the Raman fiber laser (black dashed line) and its numerical reproduction using the Van-noise (gray line).

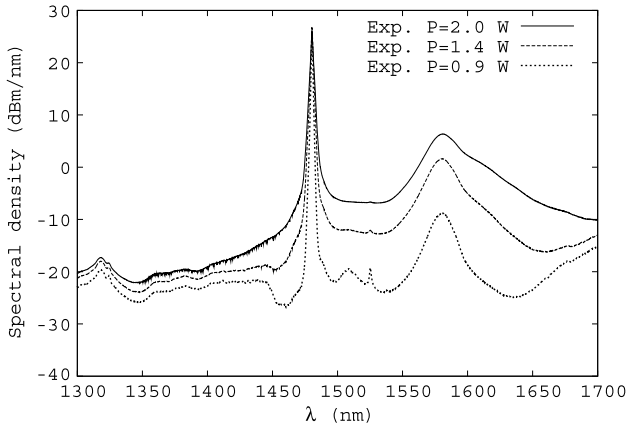


Fig. 3. Spectral output after propagation in 800 m of the HNLF for several input powers.

available attenuators, the maximum injected optical power was 2 W. All the spectra have a hump centered around 1580 nm that is easily recognized as the Stokes band of the SRS since it is frequency shifted from the pump by 13 THz. In fact, the onset of this Stokes spectral band was already referred as the dominant effect on SCG pumped with CW signals in the normal dispersion [23,24]. The Stokes band for the input power of 2 W has a long wavelength tail and, since it lies in the anomalous GVD, that may indicate the generation of solitonic kind of pulses that then red-shift by intrapulse Raman scattering. The spectral level in between the pumps and the Stokes band is relatively higher and it may be explained by FWM effects since it lies in the ZDW region of the fiber where phase matching is obtained more easily.

In order to use the actual Raman response of the fiber, the Raman gain was measured. Figure 4 shows the Raman gain coefficient over the mode effective area as obtained from Raman decibel gain measurements with pump on and pump off, $G$, through the relation [25]

$$G(\Omega) = 10\log_{10}\frac{P^{\mathrm{on}}(f)}{P^{\mathrm{off}}(f)} = \frac{4.343 g_R P_0 L_{\mathrm{eff}}}{k A_{\mathrm{eff}}}, \qquad (1)$$

where $P^{\mathrm{on}}(f)$ is the power at frequency $f = f_{\mathrm{pump}} + \Omega$ obtained with the pump signal on and $P^{\mathrm{off}}(f)$ with the pump

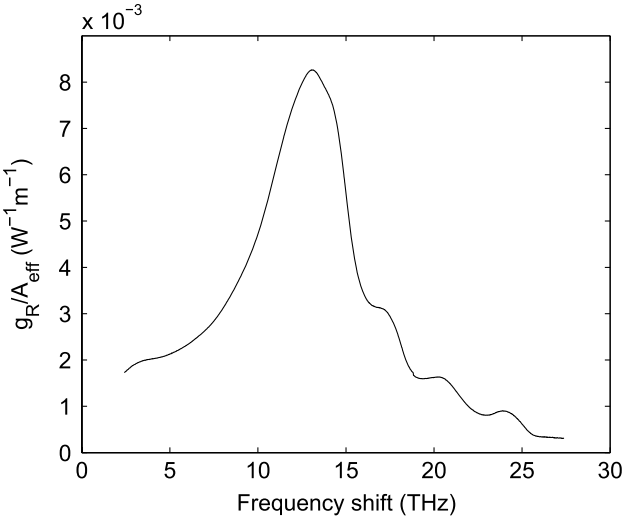


Fig. 4. Raman gain coefficient over effective area of the fiber versus frequency shift.

signal off. The input power pump is $P_0$ and $k$ is a parameter that accounts for the polarization state of the pump; it is 1 for linearly polarized pump and 2 for depolarized pump. $L_{\text{eff}}$ is the effective length given by $L_{\text{eff}} = (1 - \exp(-\alpha L))/\alpha$, where $L$ is the fiber length.

## 3. NUMERICAL MODEL

### A. Propagation Equation

In order to simulate the propagation of the depolarized CW signal along the fiber, we have used two coupled GNLSEs as follows [25–27]

$$\frac{\partial A_x}{\partial z} + \frac{i}{2}\beta_2\frac{\partial^2 A_x}{\partial t^2} - \frac{1}{6}\beta_3\frac{\partial^3 A_x}{\partial t^3} = -\frac{\alpha}{2}A_x + i\gamma(1-f_R)(|A_x|^2A_x + \frac{2}{3}|A_y|^2A_x + \frac{1}{3}A_x^*A_y^2) + i\gamma f_R\Big\{A_x\int_0^\infty([f_a h_a(t') + f_b h_b(t')]|A_x(t-t')|^2 + f_a h_a(t')|A_y(t-t')|^2)\mathrm{d}t' + \frac{1}{2}A_y\int_0^\infty f_b h_b(t')[A_y^*(t-t')A_x(t-t') + A_y(t-t')A_x^*(t-t')]\mathrm{d}t'\Big\}, \quad (2)$$

which is the propagation equation for the signal envelope $A_x$ of the optical field. A similar equation stands for component $A_y$. The amplitudes $A_x$ and $A_y$ represent the polarization components of the optical field in units of square root of power; $z$ and $t$ are the propagation distance and a retarded time that propagates at the group velocity which is assumed equal for both polarizations; $\beta_i$ $(i = 2, 3)$ are the dispersion parameters given by $\partial^i\beta/\partial\omega^i$ where $\beta$ is the propagation constant at the central frequency $\omega_0$ and $\alpha$ is the loss coefficient. The nonlinear response is of two different kinds, the Kerr response that is an instantaneous response and the Raman response that is noninstantaneous. The nonlinear parameter $\gamma$ is given by $\gamma = \omega_0 n_2/cA_{\text{eff}}$ where $n_2$ is the nonlinear refractive index, $c$ is the vacuum light velocity, and $A_{\text{eff}}$ is the optical mode effective area. The nonlinear parameter embraces both Kerr and Raman responses and $f_R$ is the ratio of Raman nonlinear parameter $\gamma_R$ and $\gamma$, i.e., $f_R = \gamma_R/\gamma$. The functions $h_a(t)$ and $h_b(t)$ are nonzero only for $t > 0$ and normalized such that their total integral over $t$ is unitary. The imaginary part of their Fourier transforms may be directly obtained from the parallel and perpendicular Raman gain [27,28]

$$\frac{g_\parallel}{A_{\text{eff}}} = 2\gamma_R\,\mathrm{Im}(f_a\tilde{h}_a(\Omega) + f_b\tilde{h}_b(\Omega)), \qquad \frac{g_\perp}{A_{\text{eff}}} = \gamma_R f_b\,\mathrm{Im}(\tilde{h}_b(\Omega)).$$

The parameters $f_a$ and $f_b$ obey the relation $f_a + f_b = 1$. Note that for large pulses the convolution is approximately of the same form as the Kerr term such that, if the light is linearly polarized, we obtain a term of the form $\gamma|A_x|^2A_x$.

Since we have only experimental data for the total Raman gain, we surpass this difficulty by assuming that the perpendicular Raman gain is negligible, i.e., $f_b = 0$ and $f_a = 1$, in which case the above equation reduces to

$$\frac{\partial A_x}{\partial z} + \frac{i}{2}\beta_2\frac{\partial^2 A_x}{\partial t^2} - \frac{1}{6}\beta_3\frac{\partial^3 A_x}{\partial t^3} = -\frac{\alpha}{2}A_x + i\gamma(1-f_R)(|A_x|^2A_x + \frac{2}{3}|A_y|^2A_x + \frac{1}{3}A_x^*A_y^2) + i\gamma f_R A_x\int_0^\infty h_a(t')[|A_x(t-t')|^2 + |A_y(t-t')|^2]\mathrm{d}t' \quad (3)$$

and $h_a(t)$ and $f_R$ can be evaluated from the experimental Raman gain data that we present in Fig. 4. In fact, the imaginary part of the Fourier transform of $h_a(t)$ may be obtained as follows:

$$\frac{g_R(\Omega)}{A_{\text{eff}}} = 2\gamma_R\,\mathrm{Im}(\tilde{h}_a(\Omega)), \quad (4)$$

where the real part of $\tilde{h}_a(\Omega)$ was obtained using a Hilbert transform and $h_a(t)$ by an inverse Fourier transform (see Fig. 5). An unitary full integral for $h_a(t)$ was guaranteed and the $\gamma_R$ and consequently $f_R$ were evaluated. The parameters of the fiber at $\lambda = 1480$ nm are compiled in Table 1.

### B. Input-Noise Model

We have done a preliminary study using noise as dictated by the one photon per mode model [14] and the standard phase-diffusion model [13,18] that retrieves a Lorentzian spectrum. However, those models do not reproduce the power spectral density of the actual laser or the output power spectral density, as may be observed in Fig. 8. Thus, and throughout the rest of the work, we used random spectral amplitude and phase following the approach presented in [21], which may replicate any power spectrum density irrespective of its theoretical or experimental nature. Moreover, we compare the results with the ones for random inputs with similar characteristics, that is, also exhibiting amplitude and phase fluctuations and having a given power spectral density, but originating from an adjustment of the phase-diffusion model [19]. In this paper, we will call these two latter types of input-noise model by Van-noise and F-noise, respectively.

The model based on [21] was already used by one of the authors in another context [29] and is here sketched. Let us suppose that our CW signal emits linear depolarized light possessing a power spectral density given by $G(\omega)$ and that may be decomposed into two equal amplitude polarizations. This signal may be modeled as a collection of a large number of independent radiators, each emitting at certain frequency, with a certain phase and amplitude. By taking the optical field of the radiator $j$ emitting at $\omega_n$ to be

$$A_j\,\exp(-i\omega_n t + i\phi_j),$$

the total optical field at frequency $\omega_n$ is

$$A_n(t) = \sum_j A_j\,\exp(-i\omega_n t + i\phi_j) = Z_n\,\exp(-i\omega_n t),$$

with

$$Z_n = a_n + ib_n = \sum_j A_j(\cos\phi_j + i\,\sin\phi_j).$$

Assuming that the phase is uniformly distributed in the interval $[0, 2\pi)$ and that the number of radiators emitting at $\omega_n$ is large, $a_n$ and $b_n$ are independent Gaussian random variables with zero mean and variance given by

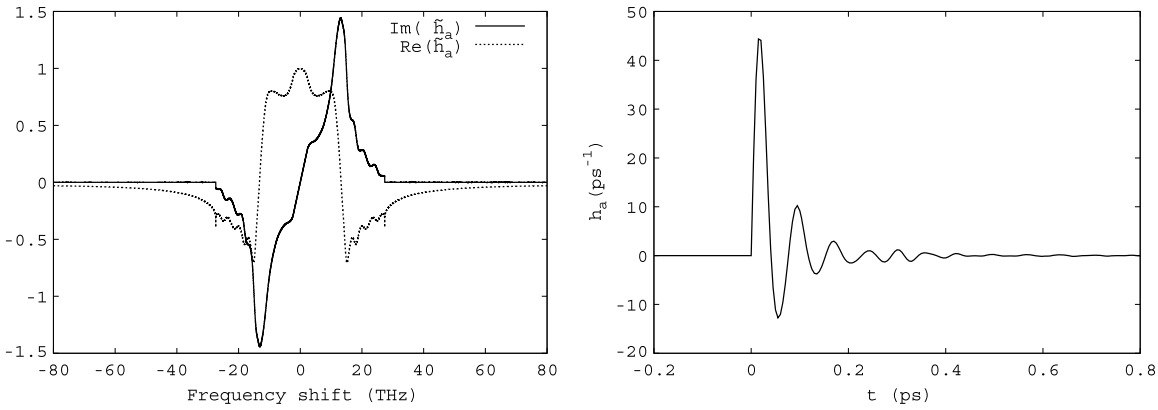


Fig. 5. Normalized Raman (a) spectral and (b) temporal responses.

**Table 1. Fiber Parameters for $\lambda = 1480$ nm**

| $\beta_2$ (ps$^2$ km$^{-1}$) | $\beta_3$ (ps$^3$ km$^{-1}$) | $\gamma$ (W$^{-1}$ km$^{-1}$) | $f_R$ | $\alpha$ (Npkm$^{-1}$) | $L$ (m) |
|---|---|---|---|---|---|
| 1.09 | 0.0229 | 10.5 | 0.293 | 0.725 | 800 |

$\sigma_n^2 = \bar{a}_n^2 = \bar{b}_n^2 = G(\omega_n)\Delta\omega/2$. The total field is given by the sum of the optical field for every frequency, that is

$$A(t) = \sum_{n=-N/2}^{N/2} Z_n \exp[-i(\omega_0 t + n\Delta\omega t)] = \tilde{Z}(t)\exp(-i\omega_0 t)$$

where $\tilde{Z}(t)$ and $Z_n$ are Fourier transforms of each other, such as

$$\tilde{Z}(t) = \sum_{n=-N/2}^{N/2} Z_n \exp(-in\Delta\omega t).$$

Hence, we have started with the power spectral density of our Raman fiber laser as represented in Fig. 2 and generated two sets of random numbers with a Gaussian distribution with zero average and unitary variance. Then, we transform them to $a_n$ and $b_n$ according to $\bar{a}_n^2 = \bar{b}_n^2 = G(\omega_n)\Delta\omega/2$. Finally, we

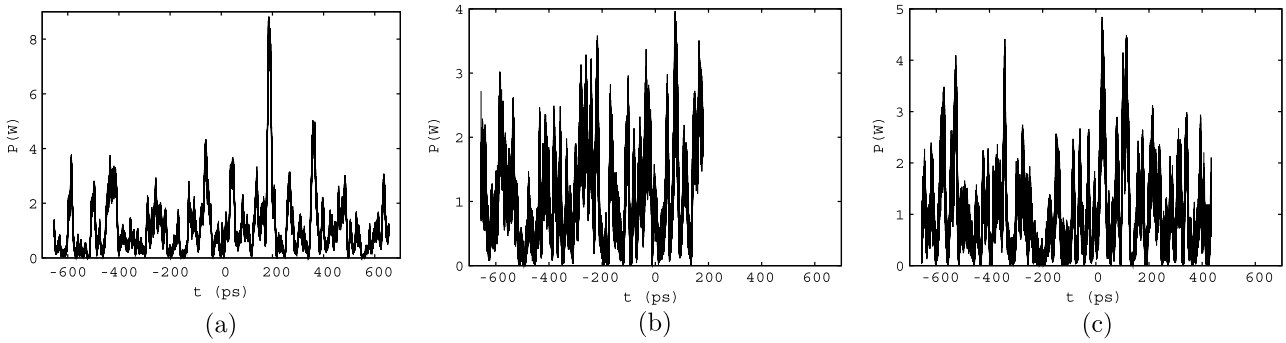


Fig. 6. Example of power profiles for an average power of 1 W: (a) Van-noise, (b) F-noise with Lorentzian linewidth equal to the estimated linewidth of the Raman laser PSD, and (c) F-noise with linewidth 10 times larger.

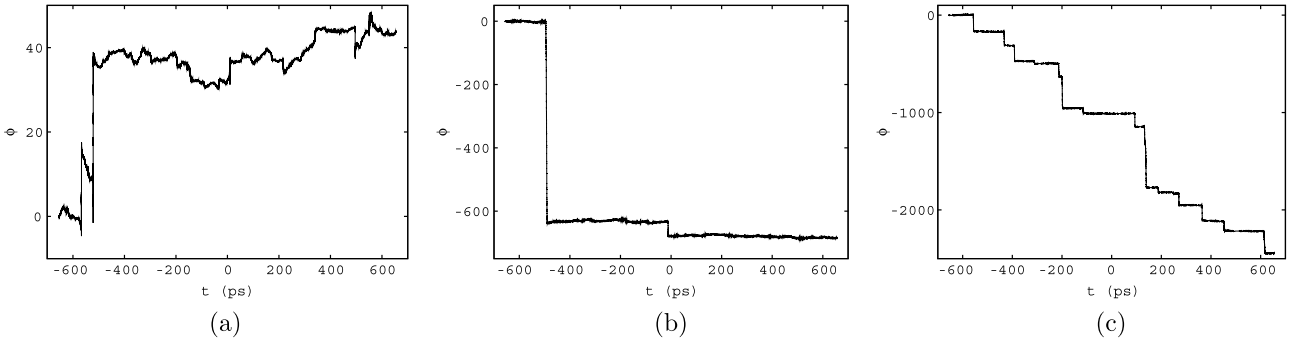


Fig. 7. Phase profiles of the signals whose power profiles are shown in Fig. 6.

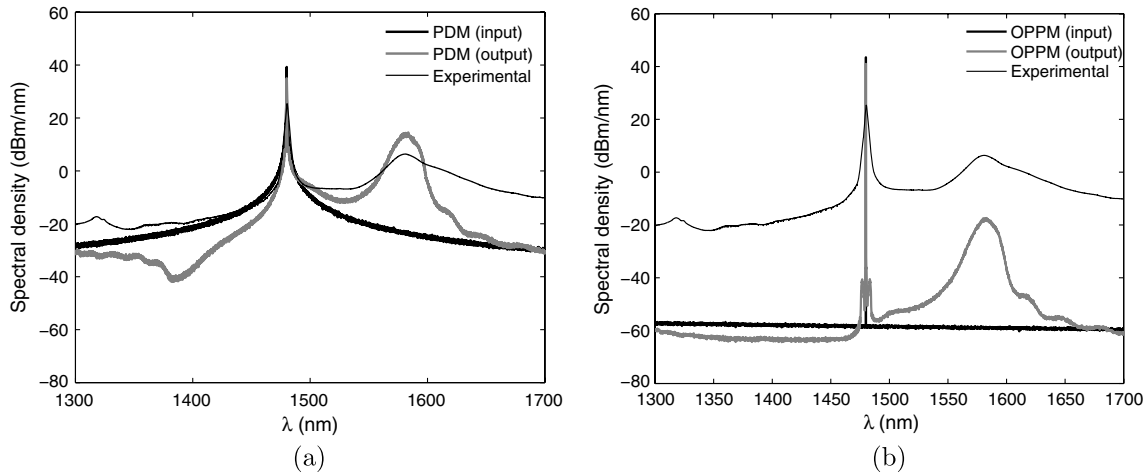


Fig. 8. Input and output spectra for 2 W and two input noise models: (a) PDM (phase diffusion model) and (b) OPPM (one photon per mode).

obtained the optical amplitude in time, $\tilde{Z}$, applying a Fourier transform to $Z_n$. The amplitude $\tilde{Z}(t)$ is proportional to the amplitudes $A_x$ and $A_y$ in Eq. (3). We have used different random noise for each of the field polarizations. In the same Fig. 2, the curve labeled as numerical was obtained by averaging 10 input random signals created with this noise-input model. Graphs in Figs. 6(a) and 7(a) show the intensity and phase of one run of this noise model.

As mentioned above, the F-noise originates from random inputs obtained from the phase diffusion model. According to this model, the random signal is a constant amplitude signal with a phase that is the integral of random frequency fluctuations. The random frequency is assumed to be a zero mean Gaussian white noise, with a variance that depends on the laser linewidth and the bandwidth associated with the finite numerical time and frequency windows considered [18]. As a result, the random signal has a Lorentzian power spectrum shape, with the same linewidth as the CW laser. Then, this Lorentzian power spectrum can be reshaped into any desired form, allowing the exact reproduction of the power spectral

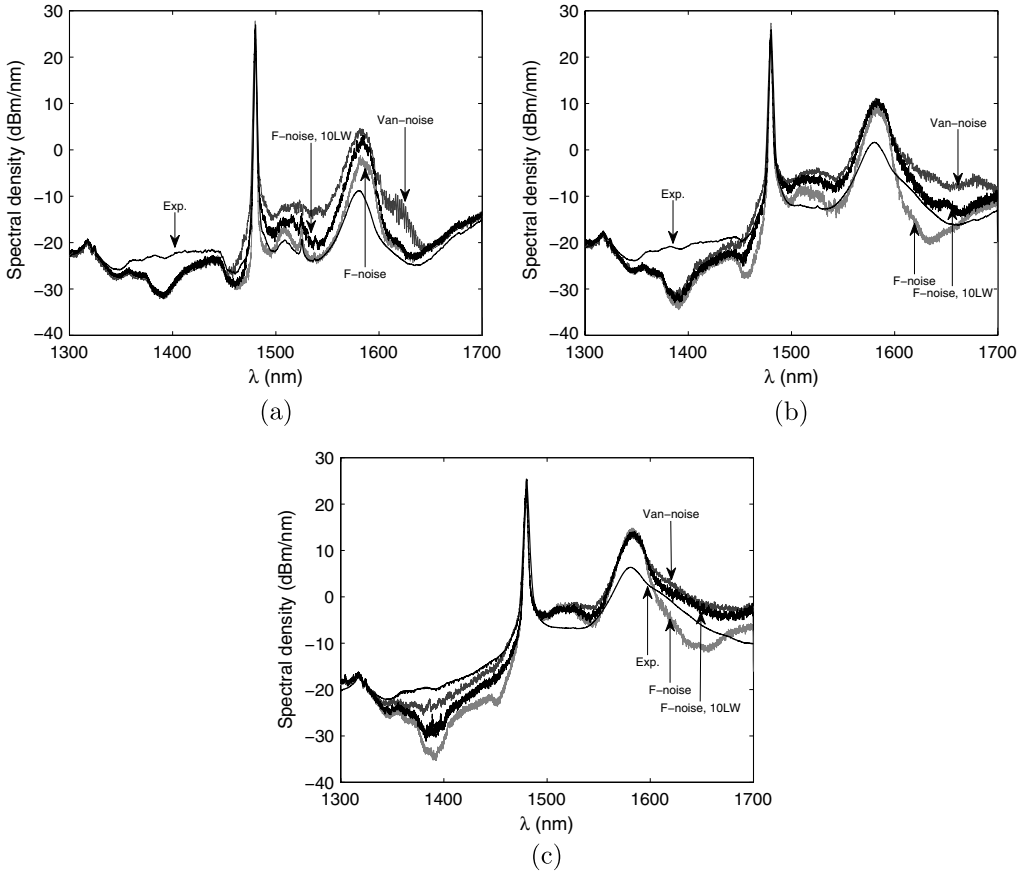


Fig. 9. Comparison of experimental and numerical results using both Van-noise and F-noise for (a) 0.9 W, (b) 1.4 W, and (c) 2.0 W. F-noise was used with two choices for the width of the backing Lorentzian.

density of any source [19]. Note that, by exact reproduction, we mean that every random input signal has exactly the same power spectral density that is equal to the original that we intend to reproduce. It should be pointed out that the reshaping process of the Lorentzian power spectrum also implies a change in the temporal characteristics of the random signal, with this signal no longer possessing constant amplitude but, instead, exhibiting fast fluctuations in both amplitude and phase. Moreover, as Figs. 6(b), 6(c) and 7(b), 7(c) show, the amplitude of these rapid oscillations strongly depends on the similarity between the linewidths of the intermediate Lorentzian spectrum and of the final power spectrum. This suggests that a careful choice of the Lorentzian linewidth is required in order to correctly model a given power spectrum.

The numerical simulations were done on a temporal window of 1.3 ns with $2^{18}$ discrete points. The power spectrum densities were estimated using the periodogram smoothed over 16 adjacent discrete frequencies and averaged over 10 different simulations with different random noise in order to emulate the OSA integration times.

## 4. COMPARISON OF EXPERIMENTAL AND NUMERICAL RESULTS

The numerical results are compared to the experimental results in Figs. 8 and 9. Figure 8 compares the experimental output spectra for input power of 2 W with the results of simulations using one photon per mode and the standard phase diffusion model. Both simulated spectra exhibit the Stokes band but their profiles differ significatively from the experimental profile. Moreover, the result obtained with one photon per mode shows a power level that is 35 dBm lower than the experimental one. The agreement is substantially increased if the F-noise and Van-noise are used. Generally, the transfer of power from the pump at 1480 nm to the Stokes band is larger in the numerical results. For the input power of 0.9 W, all the numerical results conform with the experimental Stokes band, but the curve correspondent to the F-noise that uses a backing Lorentzian spectrum with the same width as estimated on the experimental spectrum is closer to the experimental power level. On the other hand, for larger input powers 1.4 and 2 W, this same input-noise model gives the output spectra that most disagree with the experimental one. The F-noise using a Lorentzian 10 times larger than the laser spectrum and the Van-noise give identical results and the agreement is especially good for 2 W. Another feature of the output spectra that is present in the numerical results and absent from the experimental results is a depression around 1380 nm. The depression in the numerical results may be understood as inverse Raman scattering, that is, the absorption of radiation that has frequencies in the anti-Stokes band. Our explanation for the absence of this feature in the experimental

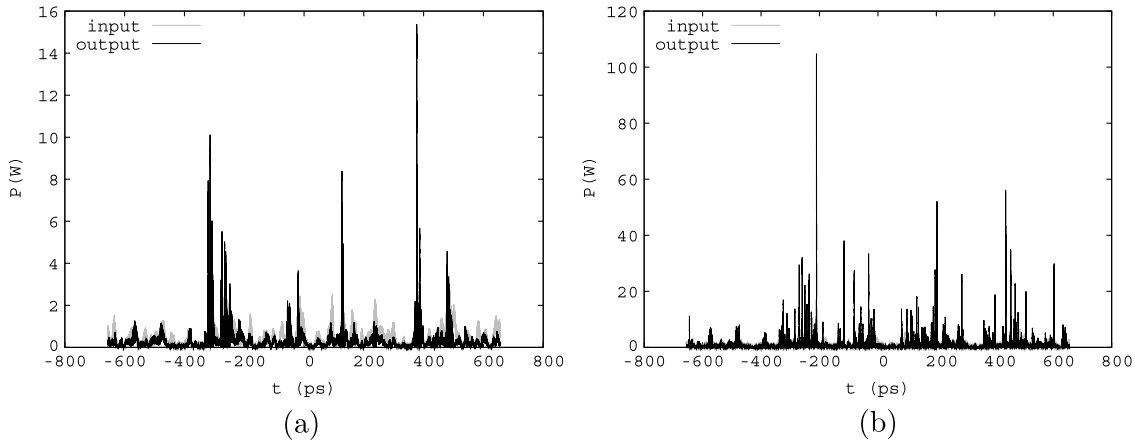


Fig. 10. Example of input and output power profiles for the Van-noise and (a) 0.9 W and (b) 2 W. The line correspondent to the input is somehow hidden behind the output line.

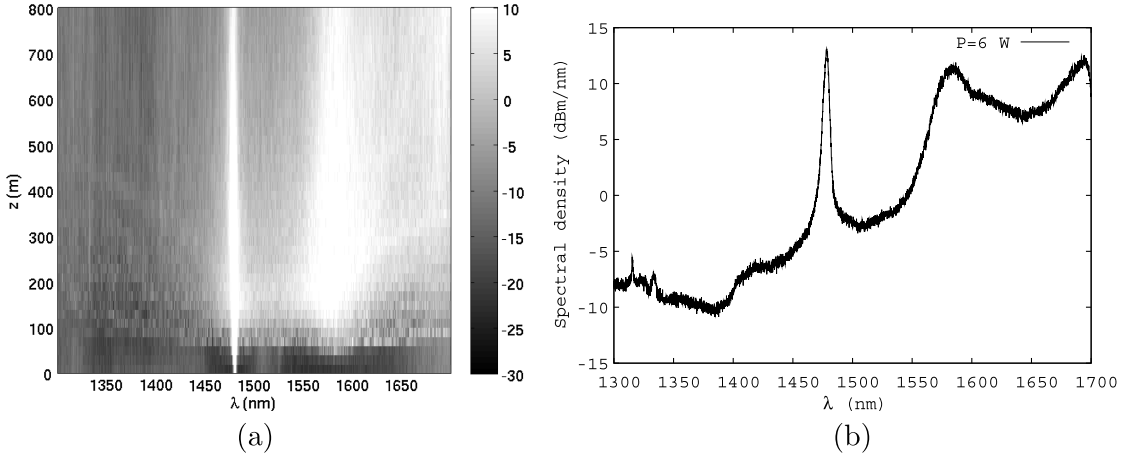


Fig. 11. Spectral evolution and final spectrum as simulated for a Van-noise input power of 6 W and 800 m of the HNLF.

output spectrum is the occurrence of parametric amplification of this anti-Stokes band in a process similar to the one described in [30] and that may be phase matched in the actual fiber. Note that the numerical simulations use dispersion coefficients up to third order consistent with dispersion data that was experimentally obtained in the wavelength range 1495–1640 nm. In fact, the experimental dispersion in this wavelength range is well fitted to a line, but the dispersion curve is possibly significantly different from this line outside this wavelength region. It may be the case that the actual linear phase mismatch between the anti-Stokes band and the pump is similar to the nonlinear mismatch contribution, such that parametric amplification balances inverse Raman scattering and the anti-Stokes band stays at the same level as its surrounding. The fact that the difference in power density at this band on numerical and experimental results is power dependent is in favor of our argument.

In Section 2, we indicated that the larger Stokes band for larger input powers should be due to the generation of solitons. In order to support that hypothesis, we have observed the temporal output profiles for 0.9 and 2 W. Example of those profiles are shown in Fig. 10. In fact, for 2 W, the intense peaks are much more frequent than in the 0.9 W case.

We have further increased the pump power in the simulations and achieved reasonable output power covering the $C + L$ telecommunication bands using input power of 6–7 W. The spectral evolution of the signal for an input power of 6 W is shown in Fig. 11(a) and the output spectra in Fig. 11(b). For input powers larger than 7 W (up to 10 W), the simulations showed that the spectral regions benefiting from that would be outside the telecommunication wavelength region.

## 5. CONCLUSIONS

We presented experimental data showing spectral broadening as result of propagation of a CW signal on a HNLF in the normal dispersion regime. The experiment was simulated using coupled GNLSEs using dispersion coefficients, nonlinear parameter, and the actual Raman response of the fiber that were experimentally determined. Also, the CW signal in the time domain was estimated using various input-noise models. Two of those models reproduce the actual power spectral density of the laser and provided better agreement with the experimental results. Among those two, the one proposed here for SCG simulations has been shown to be less arbitrary since it does not depend on the characteristics of any backing Lorentzian spectrum. The output spectra obtained with this input-noise were reasonably close to the experimental results. The model was also used to predict further enhancement of the spectral broadening for other experimental conditions.

## ACKNOWLEDGMENTS

This work was partially supported by the Fundação para a Ciência e Tecnologia, FCT, European Union FEDER program, and PTDC programs, through the projects PTDC/EEA-TEL/105254/2008 (OSP-HNLF), PTDC/FIS/112624/2009 (CONLUZ), and PEst-C/CTM/LA0025/2011.

## REFERENCES

1. R. R. Alfano and S. L. Shapiro, "Emission in the region 4000 to 7000 a via fourphoton coupling in glass," Phys. Rev. Lett. **24**, 584587 (1970).
2. J. K. Ranka, R. S. Windeler, and A. J. Stentz, "Visible continuum generation in air silica microstructure optical fibers with anomalous dispersion at 800 nm," Opt. Lett. **25**, 25–27 (2000).
3. D. R. Solli, B. Jalali, and C. Ropers, "Seeded supercontinuum generation with optical parametric down-conversion," Phys. Rev. Lett. **105**, 233902 (2010).
4. S. P. Stark, A. Podlipensky, N. Y. Joly, and P. S. J. Russell, "Ultraviolet-enhanced supercontinuum generation in tapered photonic crystal fiber," J. Opt. Soc. Am. B **27**, 592–598 (2010).
5. E. J. R. Kelleher, J. C. Travers, S. V. Popov, and J. R. Taylor, "Role of pump coherence in the evolution of continuous-wave supercontinuum generation initiated by modulation instability," J. Opt. Soc. Am. B **29**, 502–512 (2012).
6. B. Washburn and N. Newbury, "Phase, timing, and amplitude noise on supercontinua generated in microstructure fiber," Opt. Express **12**, 2166–2175 (2004).
7. J. M. Dudley, G. Genty, and S. Coen, "Supercontinuum generation in photonic crystal fiber," Rev. Mod. Phys. **78**, 1135–1184 (2006).
8. Y. Han and B. Jalali, "Photonic time-stretched analog-to-digital converter: fundamental concepts and practical considerations," J. Lightwave Technol. **21**, 3085–3103 (2003).
9. G. Busch, R. Jones, and P. Rentzepis, "Picosecond spectroscopy using a picosecond continuum," Chem. Phys. Lett. **18**, 178–185 (1973).
10. D. L. Marks, A. L. Oldenburg, J. J. Reynolds, and S. A. Boppart, "Study of an ultrahigh-numerical-aperture fiber continuum generation source for optical coherence tomography," Opt. Lett. **27**, 2010–2012 (2002).
11. J. M. Dudley, L. Provino, N. Grossard, H. Maillotte, R. S. Windeler, B. J. Eggleton, and S. Coen, "Supercontinuum generation in air–silica microstructured fibers with nanosecond and femtosecond pulse pumping," J. Opt. Soc. Am. B **19**, 765–771 (2002).
12. G. Genty, M. Lehtonen, H. Ludvigsen, and M. Kaivola, "Enhanced bandwidth of supercontinuum generated in microstructured fibers," Opt. Express **12**, 3471–3480 (2004).
13. A. Mussot, E. Lantz, H. Maillotte, T. Sylvestre, C. Finot, and S. Pitois, "Spectral broadening of a partially coherent cw laser beam in single-mode optical fibers," Opt. Express **12**, 2838–2843 (2004).
14. S. M. Kobtsev and S. V. Smirnov, "Modelling of high-power supercontinuum generation in highly nonlinear, dispersion shifted fibers at CW pump," Opt. Express **13**, 6912–6918 (2005).
15. F. Vanholsbeeck, S. Martin-Lopez, M. Gonzalez-Herraez, and S. Coen, "The role of pump incoherence in continuous-wave supercontinuum generation," Opt. Express **13**, 6615–6625 (2005).
16. A. E. El-Taher, J. D. Ania-Castañón, V. Karalekas, and P. Harper, "High efficiency supercontinuum generation using ultra-long raman fiber cavities," Opt. Express **17**, 17909–17915 (2009).
17. A. K. Abeeluck and C. Headley, "Supercontinuum growth in a highly nonlinear fiber with a low-coherence semiconductor laser diode," Appl. Phys. Lett. **85**, 4863–4865 (2004).
18. M. H. Frosz, O. Bang, and A. Bjarklev, "Soliton collision and raman gain regimes in continuous-wave pumped supercontinuum generation," Opt. Express **14**, 9391–9407 (2006).
19. M. H. Frosz, "Validation of input-noise model for simulations of supercontinuum generation and rogue waves," Opt. Express **18**, 14778–14787 (2010).
20. J. Travers, S. Popov, and J. Taylor, "A new model for cw supercontinuum generation," in *Lasers and Electro-Optics, 2008 and 2008 Conference on Quantum Electronics and Laser Science* (IEEE, 2008), pp. 1–2.
21. G. Vannucci and M. C. Teich, "Computer simulation of superposed coherent and cahotic radiation," Appl. Opt. **19**, 548–553 (1980).
22. N. Silva, N. Muga, and A. Pinto, "Effective nonlinear parameter measurement using fwm in optical fibers in a low power regime," IEEE J. Quantum Electron. **46**, 285–291 (2010).
23. J. Nicholson, A. Abeeluck, C. Headley, M. Yan, and C. Jørgensen, "Pulsed and continuous-wave supercontinuum generation in highly nonlinear, dispersion-shifted fibers," Appl. Phys. B **77**, 211–218 (2003).
24. A. K. Abeeluck and C. Headley, "Continuous-wave pumping in the anomalous- and normal-dispersionregimes of nonlinear fibers for supercontinuum generation," Opt. Lett. **30**, 61–63 (2005).
25. G. P. Agrawal, *Nonlinear fiber optics* (Academic, 1995).

26. C. R. Menyuk, M. N. Islam, and J. P. Gordon, "Raman effect in birefringent optical fibers," Opt. Lett. **16**, 566–568 (1991).
27. R. Hellwarth, J. Cherlow, and T.-T. Yang, "Origin and frequency dependence of nonlinear optical susceptibilities of glasses," Phys. Rev. B **11**, 964–967 (1975).
28. C. Headley III and G. P. Agrawal, "Unified description of ultrafast stimulated Raman scattering in optical fibers," J. Opt. Soc. Am. B **13**, 2170–2177 (1996).
29. M. Facão, A. Lopes, A. L. Silva, and P. Silva, "Computer simulation for calculating the second-order correlation function of classical and quantum light," Eur. J. Phys. **32**, 925–934 (2011).
30. S. Coen, S. G. Murdoch, and F. Vanholsbeeck, "Interaction of four-wave mixing and stimulated Raman scattering in optical fibers," in *Supercontinuum generation in optical fibers* (Cambridge University, 2010), pp. 199–225.